Astronomy & Astrophysics

Disk heating and bending instability in galaxies with counterrotation

Sergey Khoperskov[1,2] and Giuseppe Bertin[3]

[1] GEPI, Observatoire de Paris, CNRS, Université Paris Diderot, 5 place Jules Janssen, 92190 Meudon, France
    e-mail: `sergey.khoperskov@obspm.fr`
[2] Institute of Astronomy, Russian Academy of Sciences, 48 Pyatnitskaya st., 119017 Moscow, Russia
[3] Dipartimento di Fisica, Università degli Studi di Milano, via Celoria 16, 20133 Milano, Italy
    e-mail: `giuseppe.bertin@unimi.it`

ABSTRACT

With the help of high-resolution long-slit and integral-field spectroscopy observations, the number of confirmed cases of galaxies with counterrotation is increasing rapidly. The evolution of such counterrotating galaxies remains far from being well understood. In this paper we study the dynamics of counterrotating collisionless stellar disks by means of N-body simulations. We show that, in the presence of counterrotation, an otherwise gravitationally stable disk can naturally generate bending waves accompanied by strong disk heating across the disk plane, that is in the vertical direction. Such a conclusion is found to hold even for dynamically warm systems with typical values of the initial vertical-to-radial velocity dispersion ratio $\sigma_z/\sigma_R \approx 0.5$, for which the role of pressure anisotropy should be unimportant. We note that, during evolution, the σ_z/σ_R ratio tends to rise up to values close to unity in the case of locally Jeans-stable disks, whereas in disks that are initially Jeans-unstable it may reach even higher values, especially in the innermost regions. This unusual behavior of the σ_z/σ_R ratio in galaxies with counterrotation appears not to have been noticed earlier. Our investigations of systems made of two counterrotating components with different mass-ratios suggest that even apparently normal disk galaxies (i.e., with a minor counterrotating component so as to escape detection in current observations) might be subject to significant disk heating especially in the vertical direction.

Key words. galaxies: evolution – galaxies: kinematics and dynamics – galaxies: structure

1. Introduction

In the early stages of galactic evolution, dwarf galaxy mergers, tidal interactions with satellites, and gas accretion from cosmological filaments lead to the formation of giant disk galaxies made of stellar and/or gaseous subsystems with different angular momentum axes (Conselice et al. 2008; Davis et al. 2011; Faucher-Giguère et al. 2011; Bluck et al. 2012; Algorry et al. 2014). In such a picture, disk galaxies can be thought of as multi-spin systems (Rubin 1994; Conselice 2014). In some cases, rotation occurs in distinct planes or even in perpendicular planes, in configurations that sometimes contain structures that are usually called inner or outer polar rings (Whitmore et al. 1987; Moiseev et al. 2011; Moiseev 2012). These systems are interesting laboratories for the investigation of the dynamics of truly 3D matter distributions around galaxies (Sackett et al. 1994; Combes & Arnaboldi 1996; Khoperskov et al. 2014a). Galaxies with external elongated but inclined subsystems are rare because their dynamics would make them evolve away from such conditions (Combes & Arnaboldi 1996). The processes that lead to the formation of galaxies with subsystems rotating in the same plane are still under debate (Bertola & Corsini 1999; Corsini 2014, and references therein). It is generally believed that inclined gaseous components tend to settle into the main galactic plane, thus forming corotating or counterrotating systems (Thakar & Ryden 1996). The possibility of accretion of gas and/or stars right onto the plane of the host galaxy is not to be excluded.

On the observational side, several galaxies with strong counterrotation have been studied in detail (e.g., see Rubin et al. 1992; Sil'chenko et al. 2009; Katkov et al. 2011, 2013; Coccato et al. 2015). In turn, from the theoretical point of view, the evolutionary scenarios mentioned above suggest that such objects should not be so rare (Algorry et al. 2014). It is expected that disk galaxies of various morphological types can host a counterrotating component. The known list of confirmed cases of systems with counterrotation is often stated to contain about ten galaxies. This number is bound to increase rapidly, because of recent progress in integral-field and deep long-slit spectroscopic observations (Coccato et al. 2011; Pizzella et al. 2014; Coccato et al. 2015; Boardman et al. 2016).

The main issues that justify the great interest in galaxies characterized by counterrotation are the following:

– the origin of galaxies with counterrotation: processes of accretion of gas and/or stars;
– the observed physical properties of the counterrotating components (spatial distribution, kinematics, relative mass, stellar ages, etc.);
– dynamical and secular evolution of galaxies with counterrotation.

In this paper we focus primarily on the dynamical evolution of collisionless stellar systems with counterrotation under different initial conditions.

By means of a linear WKB (Wentzel-Kramers-Brillouin) analysis of a fluid model (Bertin & Cava 2006), it has been

shown that non-axisymmetric perturbations arise in a galactic disk when two components are rotating with different velocities, and, in particular, when the two components are in counterrotation. For a disk made of two counterrotating components, another WKB analysis showed (Lovelace et al. 1997) that the most unstable perturbations are one-armed leading waves (with respect to the rotation direction of the heavier component, assumed to be stellar) and that, in general, one-armed instabilities are more important than two-armed instabilities (see also Gulati & Deep Saini 2016, for nearly Keplerian discs). Then, by means of 2D simulations (Comins et al. 1997) it was shown that collisionless counterrotating disks, initially characterized by an axisymmetric Jeans stability parameter above unity, are subject to the formation of one-armed patterns.

Obviously, the evolution of galaxies with counterrotation is expected to depend on the parameter regime associated with the structure of the disk. Specific ways to interpret the formation of counterrotating bars (Friedli 1996; Maciejewski 2006), leading spiral structures (van Driel & Buta 1993), and other phenomena have been proposed and related to the parameter regimes that are involved. In general, it is recognized that the free energy offered by the presence of counterrotation is substantially the same as that at the basis of the so-called "two-stream instability", known and studied in a variety of contexts (Kulsrud et al. 1971; Marochnik & Suchkov 1971; Mark 1976; Bertin & Mark 1980; Bertin & Casertano 1982; Araki 1987). By means of N-body simulations, Sellwood & Merritt (1994) showed the existence of bending modes directly related to the presence of counterrotation; in their models, various structures arise which are dependent on the initial pressure anisotropy conditions. Counterrotation appears to drive the bending instability across the disk plane in a way that is similar to the driving of the Kelvin-Helmholtz instability in collisional systems in the presence of shear flows. Recently Quach et al. (2015) found that a supersonic Kelvin-Helmholtz instability can originate in the case of spatially separate counterrotating components in contact along an annular region, for which the instability is absent if the perturbation is required not to develop in the vertical direction; this suggests that one very important characteristic of the instability of counterrotating disks is its three-dimensional character. Therefore, in this paper we decided to focus, as our primary objective, on the dynamical evolution of counterrotating galaxies across the galactic plane.

Many important questions related to the evolution of counterrotating stellar disks have been addressed by Sellwood & Merritt (1994). In particular, thicker disks are expected to be more stable; because evolution usually proceeds in the direction of more stable configurations, it is natural to expect an increase of the vertical velocity dispersion during the evolution of an unstable counterrotating disk. However, it appears that a direct quantitative study of the evolution of the vertical-to-radial velocity dispersion ratio σ_z/σ_R for systems with counterrotation has not been carried out so far.

The σ_z/σ_R ratio plays an important role in the disk-halo decomposition of the kinematics of external galaxies (e.g., see The Disk Mass Project; Verheijen et al. 2004; Bershady et al. 2011), because it affects the line-of-sight velocity dispersion, whereas on the plane the σ_φ/σ_R ratio is expected to be well constrained by the epicyclic theory. In other words, knowledge or clues about the σ_z/σ_R ratio are important for the general problem of measuring the amount and distribution of dark matter in spiral galaxies.

Commonly used values for the σ_z/σ_R ratio vary in the range 0.4–0.7 (van der Kruit & de Grijs 1999). There is some growing empirical evidence that the σ_z/σ_R ratio varies monotonically with Hubble type. Namely, it is $\sigma_z/\sigma_R \approx 0.8$ for Sa-type galaxies and decreases down to ≈ 0.2 for Scd galaxies (Shapiro et al. 2003; Gerssen & Shapiro Griffin 2012). This relation has been argued to result from the impact of various mechanisms of stellar disk heating, related to: stochastic spiral patterns (Jenkins & Binney 1990; Minchev & Quillen 2006), bar structures (Saha et al. 2010), molecular cloud relaxation (Spitzer & Schwarzschild 1951; Lacey 1984; Aumer et al. 2016), disk-halo interaction (Font et al. 2001), interactions with dark-halo objects (Hänninen & Flynn 2004) or with black holes (Lacey & Ostriker 1985), heating by infalling satellites (Benson et al. 2004), and other processes (van der Kruit & Freeman 2011).

Several studies of the dynamics of thin isolated disks (without counterrotation) have shown that if the disk is too cold in the vertical direction (with $\sigma_z/\sigma_R < 0.3$) it may be subject to a kind of fire-hose instability. Early investigations were based on a linear theory (Toomre 1966; Poliachenko & Shukhman 1977; see also Kulsrud et al. 1971). This has been confirmed by many later articles, by means of analytical investigations and by N-body simulations that have also explored the conditions of instability in less idealized models (Merritt & Sellwood 1994; Sotnikova & Rodionov 2005; Khoperskov et al. 2010; Griv 2011; Rodionov & Sotnikova 2013) and extended our understanding to the nonlinear evolution of such systems. In general, it has been shown that the excited bending waves (they can be axisymmetric or non-axisymmetric) tend to heat up and to thicken the disk, so as to remove the source of instability; in some cases the σ_z/σ_R ratio has been observed to increase to values ≈ 0.7–0.9. Fire-hose related bending of stellar disks (Sellwood 1996) has also been associated with nonlinear processes during bar growth (Raha et al. 1991).

We may state that so far, in relation to the problem of disk heating and thickening, the attention has been drawn mostly to collective phenomena associated with fire-hose instabilities or spiral density waves, and the possible role of counterrotation has been either ignored or overlooked. The main goal of this paper is to find the connection between the presence of counterrotation and the vertical structure of the stellar disk. By means of high-resolution collisionless N-body simulations, we investigate the evolution of the vertical-to-radial velocity dispersion ratio σ_z/σ_R in a set of models with different masses and initial conditions for the pressure tensor.

The paper is organized as follows. In Sect. 2 we describe the models considered in our numerical simulations, especially in relation to a basic set of parameters that are expected to characterize their stability properties. In Sect. 3 we present and discuss the results of our numerical simulations. We start by considering cases without counterrotation, so as to exclude the interference of Jeans instability effects from the following runs with counterrotation (Sect. 3.1). The general evolution of models with counterrotation is described in detail in Sect. 3.2. The particular behavior related to the evolution of the σ_z/σ_R ratio is presented in Sect. 3.3. In the last two sections, Sects. 4 and 5, we address some closely related issues and summarize the results of the paper.

2. Models and parameter regimes

2.1. Setting up the simulations

We consider the full 3D dynamics of two-component stellar disks embedded in a fixed gravitational potential representing an inactive, axisymmetric dark-matter halo. We used

the N-body code described in Khoperskov et al. (2014b) where gravity force in the disk is calculated by the TreeCode Top Down algorithm (Barnes & Hut 1986). The adopted scheme of the fourth order provides a sufficiently accurate integration of the equations of the motion. The code was extensively used to resolve the issues of spiral-structures formation in pure collisionless systems (Khoperskov et al. 2012a, 2013) and in a combined N-body/hydrodynamical simulation of galaxy evolution (Khoperskov et al. 2012b, 2016). In the present work the opening angle parameter of the TreeCode algorithm is assumed to be 0.1. In physical units, the integration step is chosen to be 2×10^4 yr. We consider simulation particles of the same mass (in the range 10^3–10^4 $M_\odot$) for both components; the total number of particles is in the range 2–3×10^6.

The initialization starts from a specification of the projected density distributions Σ_1 and Σ_2, taken to be exponentially declining with R, with exponential scale lengths h_1 and h_2. The relevant gravitational forces, including the contribution of the fixed halo potential, are then computed by means of the TreeCode. At this stage we determine circular velocities and then proceed to assign the radial velocity dispersions. For each component the radial velocity dispersion $\sigma_R(R)$ is taken to have an exponential profile with scale length twice that of the corresponding projected density profile. As a result, for a single isolated disk and a choice of vertical velocity dispersion $\sigma_z \propto \sigma_R$, this would naturally lead to a vertical density profile of the $\cosh^{-2}(z/z_0)$ form, characterized by an approximately constant thickness z_0, with $z_0 = \sigma_z^2/(\pi G \Sigma)$. Obviously, when two different disk components and an external halo coexist, the relations mentioned above apply only approximately (in particular, for each component it is possible to represent the vertical density profile with an approximate $\cosh^{-2}$ profile in which the projected density determining the related thickness z_{0i} is the total density $\Sigma_{\rm tot} = \Sigma_1 + \Sigma_2$). In any case, starting from the approximate conditions listed above, the vertical equilibrium is generated with the help of a few iterations of the Jeans equations for the two components (Khoperskov et al. 2001). We are thus able to consider models that are initially characterized by various central surface densities, various exponential scale lengths, and various initial σ_z/σ_R ratios for the two disk components.

There is no evidence yet of bars and strong spirals in galaxies with counterrotation. Typically both components of galaxies with counterrotation look like lenticular galaxies (Corsini 2014). Observations suggest that the secondary (less bright) component is characterized by a line-of-sight velocity dispersion lower than that of the host component (e.g., see Katkov et al. 2016). These empirical facts are taken into consideration in our numerical models that we thus hope are sufficiently realistic. Therefore, to isolate the effects of counterrotation on the vertical disk heating, we investigate models where bar instability is suppressed.

2.2. Relative properties of the two disks

To characterize the relative properties of the two components, we follow the notation introduced by Bertin & Cava (2006; in the context of a zero-thickness two-fluid model). In particular, we define the following dimensionless parameters, in which the index 1 corresponds to the more massive host component and 2 corresponds to the secondary component:

– surface density ratio

$$\alpha \equiv \Sigma_2/\Sigma_1; \tag{1}$$

– radial velocity dispersion ("temperature") ratio

$$\beta \equiv \sigma_{R2}^2/\sigma_{R1}^2; \tag{2}$$

in general, we consider $\beta < 1$, that is, we assume that the secondary component is colder;

– angular velocity ratio

$$\delta \equiv \Omega_2/\Omega_1, \tag{3}$$

where $\delta > 0$ denotes co-rotating disks and $\delta < 0$ characterizes the case in which the secondary component is counterrotating.

2.3. Some average properties of the two-component system

To quantify the local and global heating of the two-component system in the course of the simulations, we proceed in the following way. By using radial profiles of the velocity dispersion and disk thickness we can calculate one-component radially-averaged quantities:

$$\langle X_{1,2} \rangle = \int_0^\infty 2\pi r X_{1,2}(r) \Sigma_{1,2}(r) \mathrm{d}r \Big/ \int_0^\infty 2\pi r \Sigma_{1,2}(r) \mathrm{d}r, \tag{4}$$

where X is the radial velocity dispersion σ_R, vertical velocity dispersion σ_z, vertical to radial velocity dispersion ratio σ_z/σ_R, or vertical disk thickness z; index 1 corresponds to the host component, index 2 to the secondary component.

We also introduce two-component averaged quantities:

$$\langle Y \rangle = M_{\rm tot}^{-1} \int_0^\infty 2\pi r \left[Y_1(r)\Sigma_1(r) + Y_2(r)\Sigma_2(r) \right] \mathrm{d}r \tag{5}$$

where Y is the radial velocity dispersion σ_R, vertical velocity dispersion σ_z, vertical disk thickness z, or vertical to radial velocity dispersion ratio σ_z/σ_R, and the total disk mass is:

$$M_{\rm tot} = \int_0^\infty 2\pi r [\Sigma_1(r) + \Sigma_2(r)] \mathrm{d}r. \tag{6}$$

As already noted, in the course of the simulations, when the system develops non-axisymmetric features, the above definitions are meant to include an average with respect to the azimuthal direction φ.

2.4. Parameters relevant to the development of density waves

With respect to axisymmetric density waves in a one-component disk, it is well known (Toomre 1964) that fluid and stellar disks are characterized by a similar definition of the stability parameter Q, provided that the dispersion σ that in the fluid model enters through the definition $Q = \sigma\kappa/(\pi G \Sigma)$ be replaced, in the stellar disk, by $\approx \sigma_R(\pi/3.36)$.

It is also well known that for multi-component systems the corresponding stability criterion is more complicated. Several studies have addressed the issue for various cases, given the fact that each component can be gaseous or stellar (Lin & Shu 1966; Bertin & Lin 1996; Romeo & Wiegert 2011; Romeo & Falstad 2013; Bertin 2014, and references therein). For a zero-thickness fluid model of a two-component disk (without counterrotation) the marginal stability curves in the $(\hat{\lambda}, Q_1^2)$ plane, where $\hat{\lambda}$ is

the relevant dimensionless radial wavelength of the perturbation, have been calculated for different values of the parameters (α, β) that define the density and temperature ratios of the two disks (see Eq. (16.9) in Bertin 2014). By introducing the effective stability parameter:

$$Q_{\text{eff}} = \frac{Q_1}{Q_{\max}(\alpha, \beta)}, \qquad (7)$$

where $Q_{\max}(\alpha, \beta)$ is the maximum value of the marginal stability curve, the threshold of axisymmetric Jeans instability then occurs at $Q_{\text{eff}} = 1$. In general, $Q_{\max} > 1$, because the addition of a secondary component is destabilizing. For dynamically coupled components the marginal stability curve has a single peak and its shape remains similar to that of one-component disks. On the other hand, even a light secondary component, if sufficiently cool, can have a significant impact on the stability of the combined two-component disk. In other words, each component can apparently be well on the stable side, with $Q_{1,2} > 1$, yet the combined disk can be gravitationally unstable with respect to axisymmetric Jeans instability, with $Q_{\text{eff}} < 1$. This general statement has been proved for both stellar-fluid models and fluid-fluid models. Under certain circumstances, especially when the secondary component is too cold, the two components may become dynamically decoupled, which is marked by the fact that the marginal stability curve changes shape, into a curve with two peaks.

On the other hand, with respect to non-axisymmetric density-wave perturbations (Toomre 1981; Bertin 2014, and references therein), stability depends on a second parameter, which describes the effects of a new instability mechanism related to shear (the mechanism is generally called swing or overreflection, and, for a given value of the azimuthal wavenumber m, it starts to operate when the disk is sufficiently heavy; e.g., see Eq. (15.33) in Bertin 2014). Therefore, density waves can be locally unstable even for relatively large values of Q (e.g., see Fig. 15.9 and Eq. (15.34) in Bertin 2014). In simulations with co-rotating components we then expect that, even if initialized in such a way that $Q_{\text{eff}} > 1$, some heating should occur in the plane as a result of spiral activity. In a collisionless disk this heating process may be partly limited by the presence of Lindblad resonances; however, this behavior is difficult to reproduce by means of N-body simulations, because simulations tend to lack the desired resolution in phase space. In contrast, in simulations with counterrotating disks, even if by adding a secondary component the mass of the disk is increased, the heating related to spiral activity due to overreflection may be less important, because the overreflection of non-axisymmetric waves, which relies on the presence of coherent shear, is likely to be jeopardized by the fact that the added secondary component rotates in the opposite direction with respect to the primary component.

In Fig. 1 we illustrate the radial profiles of some of the quantities defined above, for model D (characterized by counterrotation). In Table 1 we list some properties of the initial models considered in the simulations that we have performed; the last three columns provide values of the listed parameters taken at the radial location $R = R^*$ where Q_1 has its minimum.

In conclusion, for the majority of models we set up the initial parameters in such a way that $Q_{\text{eff}}(R) > 1$. We also study a case in which, during evolution, Jeans instability should coexist with the effects due to counterrotation (model C).

As to the linear stability analysis for tightly-wound non-axisymmetric perturbations in the plane of the disk related to the two-stream instability, we may refer to the study carried out by Bertin & Cava (2006) who examined the dispersion relation of a
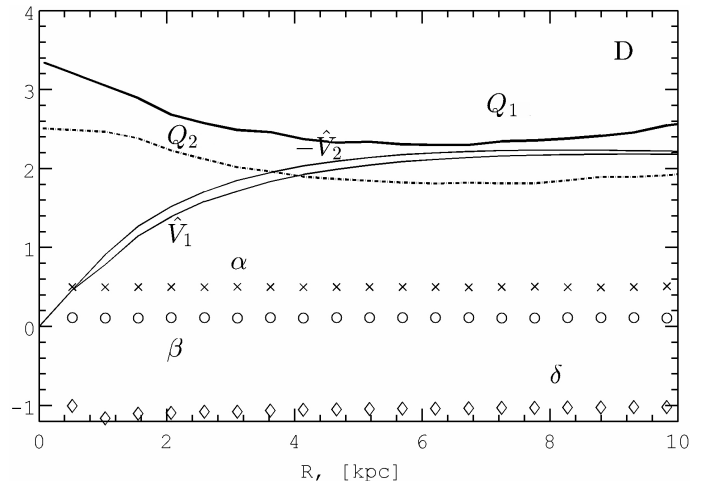

Fig. 1. Radial profiles of the initial parameters for model D (with counterrotation). The surface density ratio α, the radial temperature ratio β, the angular velocity ratio δ, and the axisymmetric stability parameters $Q_1(R)$ and $Q_2(R)$ associated with the two components. The curves $\hat{V}_{1,2}$ are the rotation curves of the two components, in units of 100 km s^{-1}.

zero-thickness two-fluid model in the WKB (tightly wound) approximation (see Eqs. (4)–(7) in that article); the general formulation makes the analysis applicable to both cases of co-rotating and counterrotating components. The analysis demonstrates that axisymmetric (i.e., $m = 0$) perturbations do not distinguish the cases of co-rotating and counterrotating components, with the stability condition given by (Eq. (7)). To compare the stability of a disk made of co-rotating components with that of a disk made of counterrotating components, we set $m \neq 0$ (and $\eta \approx 0.01$ for models with co-rotation and $\eta \approx -1.4$ for models with counterrotation), and consider the solutions of the dispersion relation (Eq. (4) in Bertin & Cava 2006). For the definition of η, see the article just cited.

In Fig. 2 we plot the imaginary parts of the solutions of the dispersion relation for pairs of models differing only in the direction of rotation of the secondary component. In the co-rotating case, only one model has a prominent unstable root (model A, $Q_{\text{eff}}(R = R^*) < 1$), which we interpret to be the result of Jeans instability. Counterrotation makes all the models locally unstable. The linear dispersion relation of each model with counterrotation has several unstable roots, dependent on the value of m (or η). The nonlinear evolution induced by all these instabilities can only be followed by means of simulations.

2.5. Issues related to the stability of bending waves

As to the properties of bending waves, linear stability analyses focusing on the role of the free energy associated with the relative motion between two components have been carried out in many papers (e.g., see Marochnik & Suchkov 1971; Bertin & Mark 1980; Bertin & Casertano 1982; Araki 1987). As with the discussion of the stability given in the previous subsection, beyond the simple realization that counterrotation has a destabilizing role, the main difficulty is to make quantitative predictions on the resulting nonlinear evolution. Therefore, we will not discuss further the related issues; instead, we proceed directly to the results of our numerical simulations.

Table 1. Initial parameters of different runs.

Model	$\Sigma_1(R=0)$	h_2	$\sigma_{R1}(R=0)$	$\sigma_{R2}(R=0)$	$\dfrac{\sigma_{z1}}{\sigma_{R1}}$	$\dfrac{\sigma_{z2}}{\sigma_{R2}}$	α	β	$Q_{max}(\alpha,\beta)$	$Q_1(R=R^*)$	$Q_{eff}(R=R^*)$
	$M_\odot\,\mathrm{pc}^{-2}$	kpc	$\mathrm{km\,s}^{-1}$	$\mathrm{km\,s}^{-1}$							
A[†]	750	3	60	35	0.5	0.5	0.5	0.34	1.8	1.44	0.8
B[†]	750	3	100	35	0.5	0.5	0.5	0.12	2.2	2.2	1.0
C	750	3	60	35	0.5	0.5	0.5	0.34	1.8	1.44	0.8
D	750	3	100	35	0.5	0.5	0.5	0.12	2.2	2.2	1.0
E	400	3	100	35	0.5	0.5	0.5	0.12	2.2	3.96	1.8
G	400	3	60	35	0.5	0.5	0.5	0.34	1.8	2.8	1.5
I01	1050	3	50	50	0.5	0.5	0.1	1	1.08	1.0	1.0
I02	970	3	50	50	0.5	0.5	0.2	1	1.2	1.2	1.0
I03	895	3	50	50	0.5	0.5	0.3	1	1.3	1.3	1.0
I04	830	3	50	50	0.5	0.5	0.4	1	1.4	1.4	1.0
I05	775	3	50	50	0.5	0.5	0.5	1	1.5	1.5	1.0
I07	660	3	50	50	0.5	0.5	0.7	1	1.7	1.7	1.0
I10	525	3	50	50	0.5	0.5	1	1	2.0	2.7	1.4
Kb	750	2	90	30	0.7	0.4	0.5	0.12	1.48	1.48	1.0
Kc	750	5	90	30	0.6	0.2	0.5	0.1	1.51	1.51	1.0

Notes. Models without counterrotation are marked by † ($\delta = 1$). Here $\Sigma_1(R = 0)$ is the central value of the surface density of the primary component, h_2 is the exponential scale length of the density distribution of the second component (for the first component, $h_1 = 3$ kpc), $\sigma_{R1}(R = 0)$ and $\sigma_{R2}(R = 0)$ are the central values of the velocity dispersion for each component, $Q_1(R = R^*)$ is the minimum value of the one-component stability parameter of the host component, and $Q_{eff}(R = R^*)$ is the effective two-component stability parameter according to Eq. (7) evaluated at R^*. Initial values of the velocity dispersion ratio for the two components are constant with radius for all models. The definitions of the density ratio α and of the temperature ratio β are given in the text; also these parameters are generally constant with radius, except for models Kb and Kc, for which the values listed here are taken at $R = R^*$, that is, the location where Q_1 has its minimum. Model I10 considers the case of exactly equal but counterrotating disks, which is unlikely to occur in real systems.
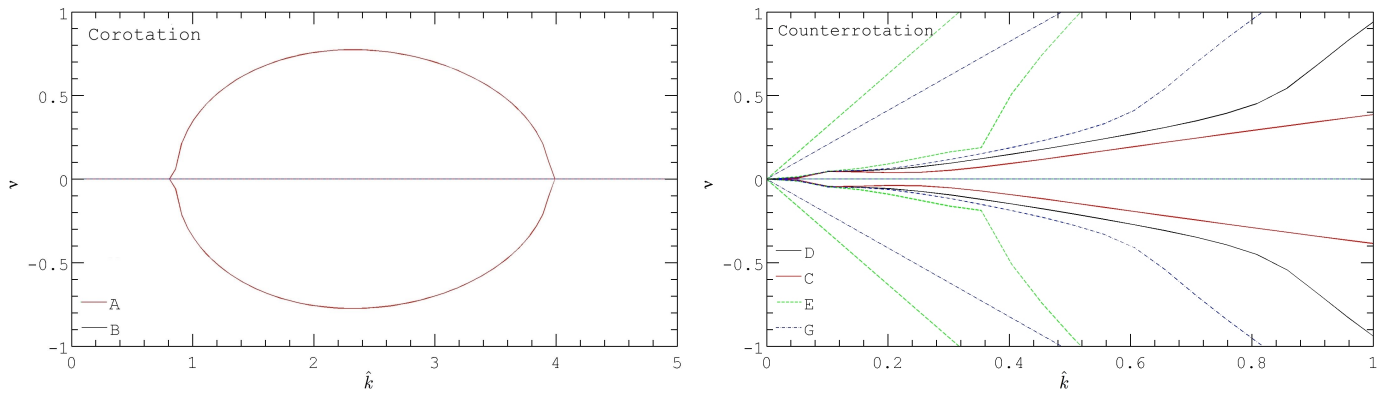

Fig. 2. Imaginary part of the solutions of the dispersion relation for two-component disks with $\eta \approx 0.01$ for models without counterrotation (*left* frame) and $\eta \approx -1.4$ with counterrotation (*right* frame), where $\hat{k}$ and ν are the relevant dimensionless radial wavenumber and the dimensionless Doppler-shifted frequency, respectively (following the notation of Bertin & Cava 2006).

3. Results of simulations

3.1. Preliminary simulations without counterrotation

Because we wish to identify effects clearly induced by the presence of counterrotation, we first consider two-component corotating disks (models A and B in Table 1) to find conditions under which the disk is reasonably free from major instabilities. The effects of possible axisymmetric instabilities in the disk plane is under control, as can be seen from Fig. 3, where we illustrate the evolution of model A (expected to be locally unstable with respect to axisymmetric perturbations, $Q_{eff}(R = R^*) = 0.8$) and model B (expected to be locally stable with respect to axisymmetric perturbations, $Q_{eff}(R = R^*) = 1.0$). The values of $Q_{eff}(R = R^*)$ should be taken as indicative only, because the

definition of this effective stability parameter is taken from a zero-thickness two-fluid model, whereas the simulations that we perform aim at describing the 3D behavior of two-component stellar disks. Because of physical mechanisms that can be traced to overreflection (or swing; see discussion in Sect. 2.4), multiple-armed spiral activity is present in both models. Figure 3 also shows the absence of bending waves. In a few rotation periods the disk heats up and evolves until phenomena "saturate" (see details in Laughlin et al. 1997; Khoperskov et al. 2012a). The disk thickens during evolution, but its vertical structure does not change much, especially in model B.

In Fig. 4 we show that for model A the radially-averaged values of the radial velocity dispersion ($\langle\sigma_{R1}\rangle$, $\langle\sigma_{R2}\rangle$, and the two-component average $\langle\sigma_R\rangle$), increases from 10–20 up to 50 $\mathrm{km\,s}^{-1}$. The radially-averaged disk thickness and velocity
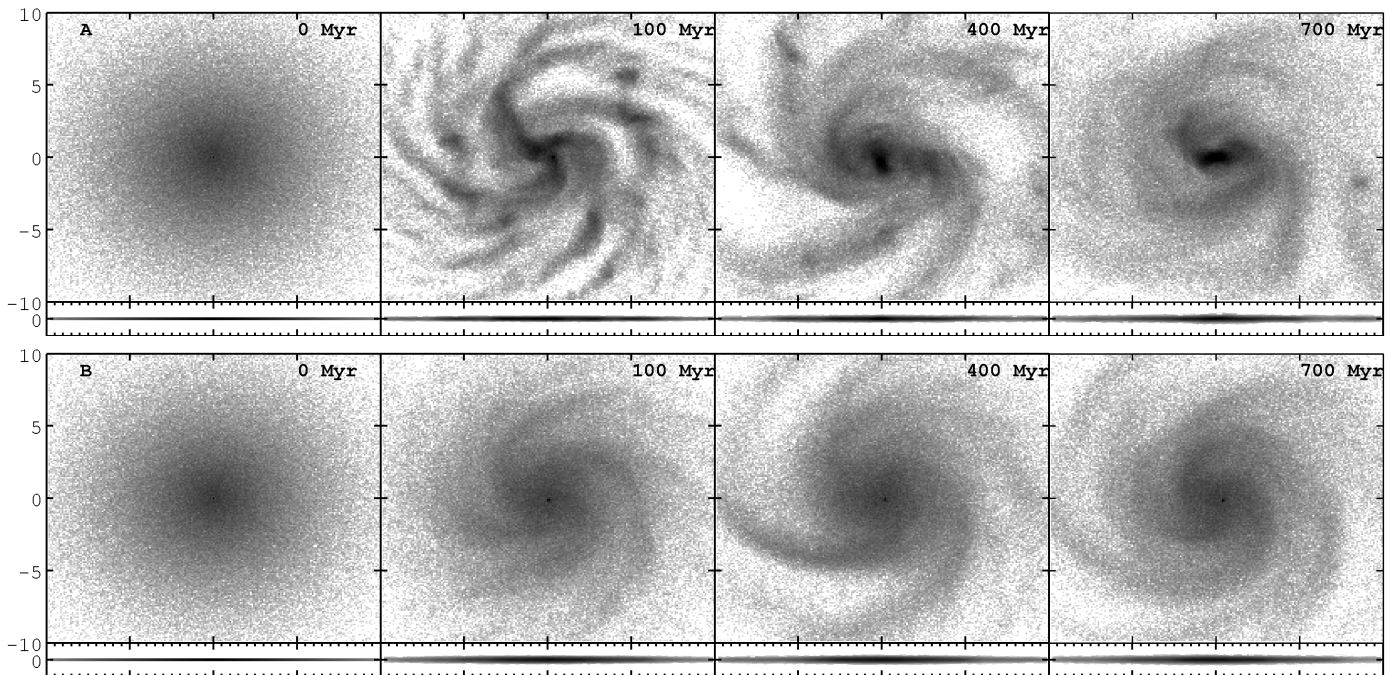
Fig. 3. Evolution of two-component co-rotating disks: *top row* illustrates the behavior of model A ($Q_{\rm eff}(R = R^*) = 0.8$), *bottom row* describes the evolution of model B ($Q_{\rm eff}(R = R^*) = 1$). Edge-on and face-on maps are shown on the same spatial scale. Face-on images have 20 kpc spatial size, vertical size of edge-on views is equal to 4 kpc.

dispersion ratio do not change significantly during the evolution even in the unstable model A. This may be due to the relatively large initial velocity dispersion ratio (0.5 for both components), well above the critical value 0.3−0.37 for (fire-hose) bending instabilities (Reshetnikov & Sotnikova 2000). We note that after several dynamical times the vertical-to-radial velocity dispersion ratio decreases as a result of heating in the plane associated with spiral density-wave activity. Such an effect is well known and has been demonstrated numerically, for example, by Gadotti & de Souza (2005), Debattista et al. (2006), Khoperskov et al. (2012a). Other two-component co-rotating disks (models F and G) are even more stable, because their effective stability parameter is larger $Q_{\rm eff}(R = R^*) \gtrsim 1.5$ (actually, for sufficiently large values of $Q_{\rm eff}(R = R^*)$ we expect that even multi-armed spiral activity would be absent). In principle, the two-component co-rotating disks might be slightly unstable, because of the possible influence of the subtle mechanism associated with the asymmetric drift explored by Bertin & Cava (2006); however, a quantitative analysis of such effects is beyond the scope of the present work.

We conclude that, when counterrotation is kept "turned-off", our models are generally free from the effects of bending instabilities and strong vertical heating. Therefore, in the following subsection we can focus on effects that we can safely attribute to the presence of counterrotation.

3.2. Simulations with counterrotation

We start by considering two-component models with disks characterized by the same parameters as those of the models described in the previous section, but in the case when the two disks are in mutual counterrotation. We pay special attention to the vertical structure of the disk.

Figures 5 and 6 show the evolution of two very different models. Model C is expected to be very unstable, because

counterrotation operates in the presence of a Jeans-unstable situation ($Q_{\rm eff}(R = R^*) = 0.8$); in turn, model E is characterized by $Q_{\rm eff}(R = R^*) = 1.8$. In both cases we observe the excitation of bending waves, as well as the formation of various structures in the face-on view of the plane.

The more unstable model exhibits the formation of a coherent one-armed spiral pattern (see Fig. 5). If referred to the rotation axis of the primary component, the observed structure is leading, which agrees with the results of the 2D simulations by Comins et al. (1997). This is likely to occur as a result of the combined effect of gravitational instability and counterrotation, because the phenomenon is not observed in model E (see Fig. 6), for which only symmetric rings are clearly seen in the face-on view of the disk. In the face-on view of model C, in addition to the dominant one-armed structure, several small-scale patterns are present in the primary component. For model C, the excitation of the bending waves starts from the center (see Fig. 5). At 200 Myr, bending waves are already seen clearly in the center, where the initially thin disk rapidly becomes thicker. Further evolution and thickening affects the outer regions. Bending waves appear to propagate with opposite phases relative to the disk plane in the two components. It is noteworthy that bending structures are very asymmetric in both components of the disk.

For the gravitationally-stable model E (see Fig. 6), we also see disk thickening and bending wave excitation. However, structures across the disk are much more symmetric than in the previous case. In the face-one view of model E there is only a ring-like structure.

Ring structures are quite surprising, because the linear WKB stability analysis of counterrotation would suggest that $m = 0$ perturbations "do not see" the presence of counterstreaming. To clarify the origin of the ring-like structures we compare snapshots of the evolution of models with various values of $Q_{\rm eff}(R = R^*)$. In Fig. 7 we show the stellar surface density distributions for models C, D, G, and E. In all models with $Q_{\rm eff}(R = R^*) \geq 1$
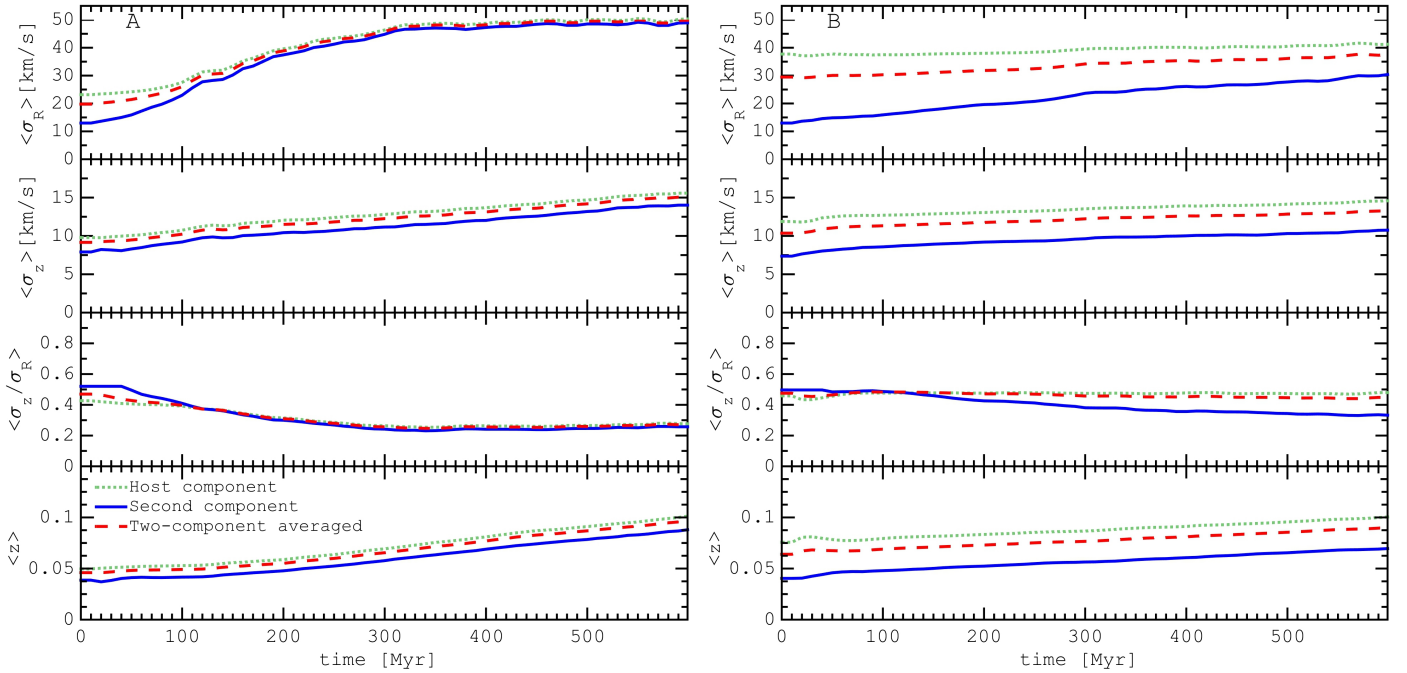
Fig. 4. Evolution of the disk parameters: radial velocity dispersion $\langle\sigma_{R1}\rangle$, $\langle\sigma_{R2}\rangle$, $\langle\sigma_{R}\rangle$ (*first row*), vertical velocity dispersion $\langle\sigma_{z1}\rangle$, $\langle\sigma_{z2}\rangle$, $\langle\sigma_{z}\rangle$ (*second row*), vertical-to-radial velocity dispersion ratio $\langle\sigma_{z1}/\sigma_{R1}\rangle$, $\langle\sigma_{z2}/\sigma_{R2}\rangle$, $\langle\sigma_{z}/\sigma_{R}\rangle$ (*third row*), and disk thickness $\langle z_1\rangle$, $\langle z_2\rangle$, $\langle z\rangle$ (*bottom row*); see Eqs. (4), (5). Blue circles correspond to the secondary (less massive) component, green crosses to the host component, and red squares represent the two-component averaged values. We recall that the two components in these models are co-rotating.

we see the presence of ring-like structures at 5–6 kpc from the center. In models with relatively low $Q_{\mathrm{eff}}(R = R^*)$ (C and D) there are also asymmetric structures, whereas in models with $Q_{\mathrm{eff}}(R = R^*) > 1$ pure ring-like structures are seen. Therefore, in our models ring formation is not expected to result from Jeans instability.

In our models rings appear to be associated with the bending waves, but actually correspond to density waves in both components (but seen better in the secondary component). In Fig. 8 we plot radial profiles of the disk thickness perturbation and surface density perturbation. For the host component, the surface density perturbations are rather small. For the secondary component, the maximum of the disk thickness perturbation approximately coincides with the bending wave maximum and for all models there is a clear peak approximately at $R = 5-6$ kpc. For the Jeans-unstable model C this peak is less prominent because of the presence of the asymmetric spiral structure. The ring-like structure is seen clearly as a maximum of the surface density perturbation, and thus it is a density wave, in all models at $R > 6$ kpc. In general, the ring is located well outside the bending wave maximum, where nonlinear effects may be more significant. Thus we conclude that, in our context, stellar rings tend to form at the outer edge of the bending wave. There is at least one observed case of a detected ring in a galaxy with counterrotation. Katkov et al. (2013) found a ring-like structure in the K-band brightness distribution of the secondary component of IC 719.

Figure 9 shows velocity dispersions and disk thickness as a function of time for four simulations with counterrotation. In contrast to the co-rotating case, there is a clear lack of growth in the radial velocity dispersion $\langle\sigma_{R1}\rangle$, $\langle\sigma_{R2}\rangle$ (in the disk plane). Only the vertical velocity dispersion increases as a result of strong nonlinear bending instability. As a general trend, this implies an increment of the velocity dispersion ratio $\langle\sigma_{z}/\sigma_{R}\rangle$ with time for all models. This growth is quite remarkable, because

the dispersion ratio can reach local values from 0.6−0.7 up to 1−1.5. We recall that for all models we assume the initial value $\sigma_{z}/\sigma_{R} = 0.5$ for both components at all radii. In the simulations we find that the constancy of the ratio breaks down for each component, because the radial profile of σ_{z}/σ_{R} exhibits a significant gradient at the end of the simulations (see black lines in the third row of each of the four panels of Fig. 9). Bending waves are known to be able also to heat up one-component galactic disks, but in a very slow process (e.g., see Rodionov & Sotnikova 2013). In contrast, two-component disk relaxation is found to occur in a very short time scale, of about 100–400 Myr.

Bending waves arise initially in the central part of the disk, forming bell-like structures that propagate to the galactic outskirts. While the vertical velocity dispersion increases with time, the radial velocity dispersion remains basically constant for both components. Only unstable model C ($Q_{\mathrm{eff}}(R = R^*) < 1$) exhibits a rather slow growth of $\langle\sigma_{R}\rangle$ in the counterrotating component (blue circles in the top left frame of Fig. 9). Such a process effectively decreases the velocity dispersion ratio $\langle\sigma_{z2}/\sigma_{R2}\rangle$ for the less massive counterrotating component, but it does not affect strongly the mean value $\langle\sigma_{z}/\sigma_{R}\rangle$ of the velocity dispersion ratio in the entire disk. In conclusion, we find that the vertical dynamics (bending waves and the resulting heating in the vertical direction) is the dominant feature of all models.

3.3. General analysis of systems with counterrotation

The above results were obtained from simulations in which the disk surface density ratio is $\alpha = 0.5$; therefore, two thirds of the total disk mass is in the host disk and one third is in the secondary, counterrotating component. To extend the parameter space, we also ran separate simulations with values of the density ratio in the range $\alpha = 0.1-1$ (see third group of models in Table 1). Then we studied two additional models (Kb and Kc),
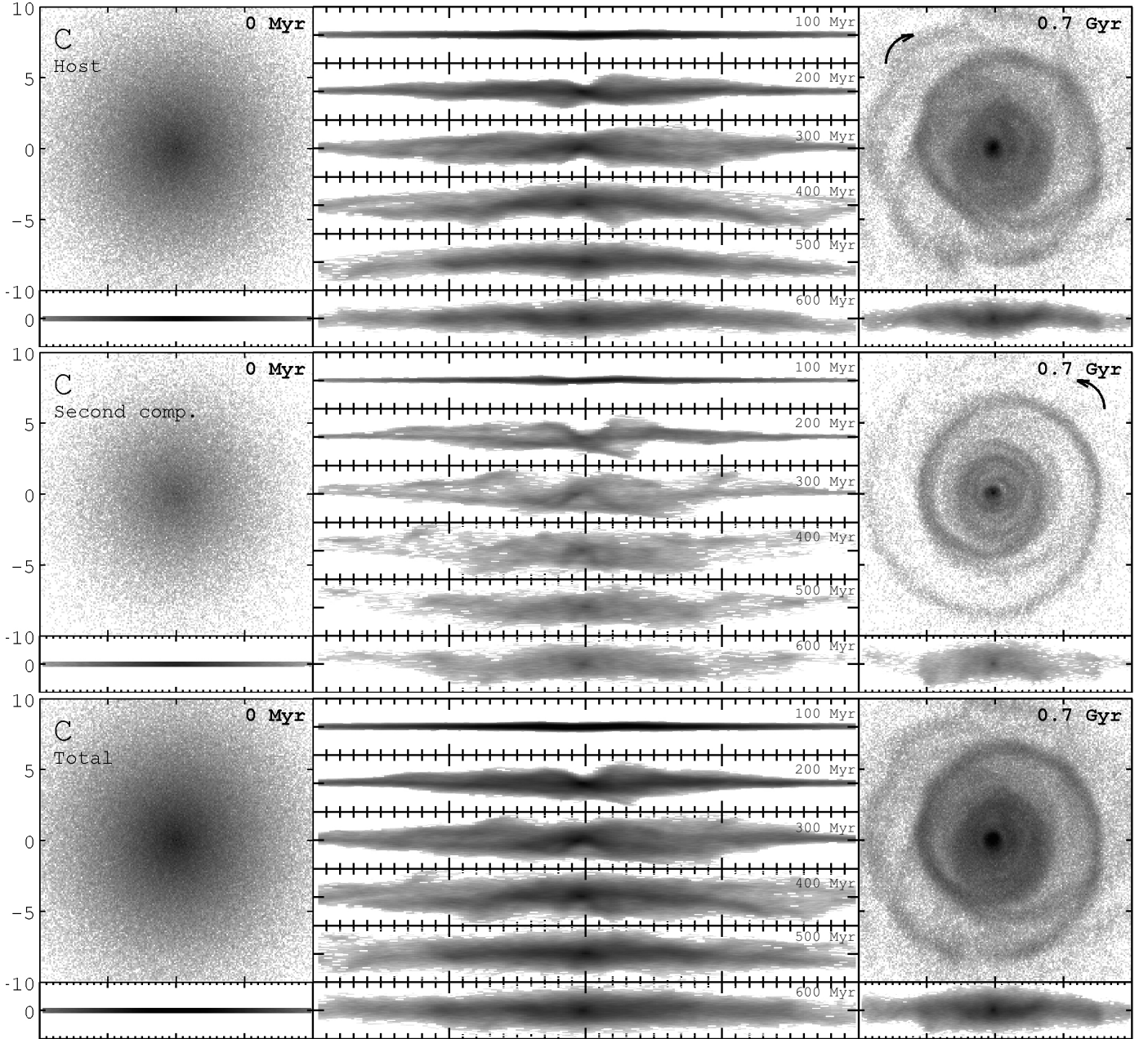
Fig. 5. Evolution of the unstable ($Q_{\mathrm{eff}}(R = R^*) = 0.8$) model C in the presence of counterrotation. In this composite figure, the top frames illustrate the evolution of the host component, *the middle frames* show the evolution of the secondary counterrotating component, and *the bottom frames* display the appearance of the disk obtained by superposition of the two components. *The left part* of the figure shows an initial snapshot of the system, whereas *the right part* illustrates the face-on morphology of the system at time $t = 0.7$ Gyr. *The central part* of the figure illustrates the time-dependent evolution of the vertical disk structure (edge-on view) in the time interval 100−600 Myr, with steps of 100 Myr. Face-on images have 20 kpc spatial size, vertical size of edge-on views is equal to 4 kpc.

with different initial values of velocity dispersion ratio for the two components (at $R = R^*$, $\sigma_{z1}/\sigma_{R1} = 0.7$, $\sigma_{z2}/\sigma_{R2} = 0.4$ for the Kb model and $\sigma_{z1}/\sigma_{R1} = 0.6$, $\sigma_{z2}/\sigma_{R2} = 0.2$ for the Kc model; see Table 1). In all these models the mean velocity dispersion ratio also increases with time up to $\langle \sigma_z/\sigma_R \rangle = 0.6$–1.2. The stability parameter $Q_{\mathrm{eff}}(R = R^*)$ for these models indicates that the disk is close to conditions of marginal stability with respect to axisymmetric perturbations in the disk plane, but this appears to be unrelated to the vertical heating, which is likely to be associated with the excitation of bending waves.

Since the vertical heating appears to be the most significant feature of our simulations in the presence of counterrotation, regularly present in most or all the models that we have considered,

we tried to see whether the amount of heating observed in the simulations tends to correlate, at the global level, with some properties of the model in its initial state. In addition to properties directly related to the parameters considered in Table 1, we decided to estimate the free energy associated with counterrotation in a two-component disk, by introducing the following dimensionless parameter, based on quantities defined in the initial state:

$$\varepsilon = \frac{\displaystyle\int_0^\infty \pi r \Sigma_2(r)[(r\Omega_2(r))^2 + \sigma_2^2(r)]\mathrm{d}r}{\displaystyle\int_0^\infty \pi r \Sigma_1(r)[(r\Omega_1(r))^2 + \sigma_1^2(r)]\mathrm{d}r} < 1 , \qquad (8)$$
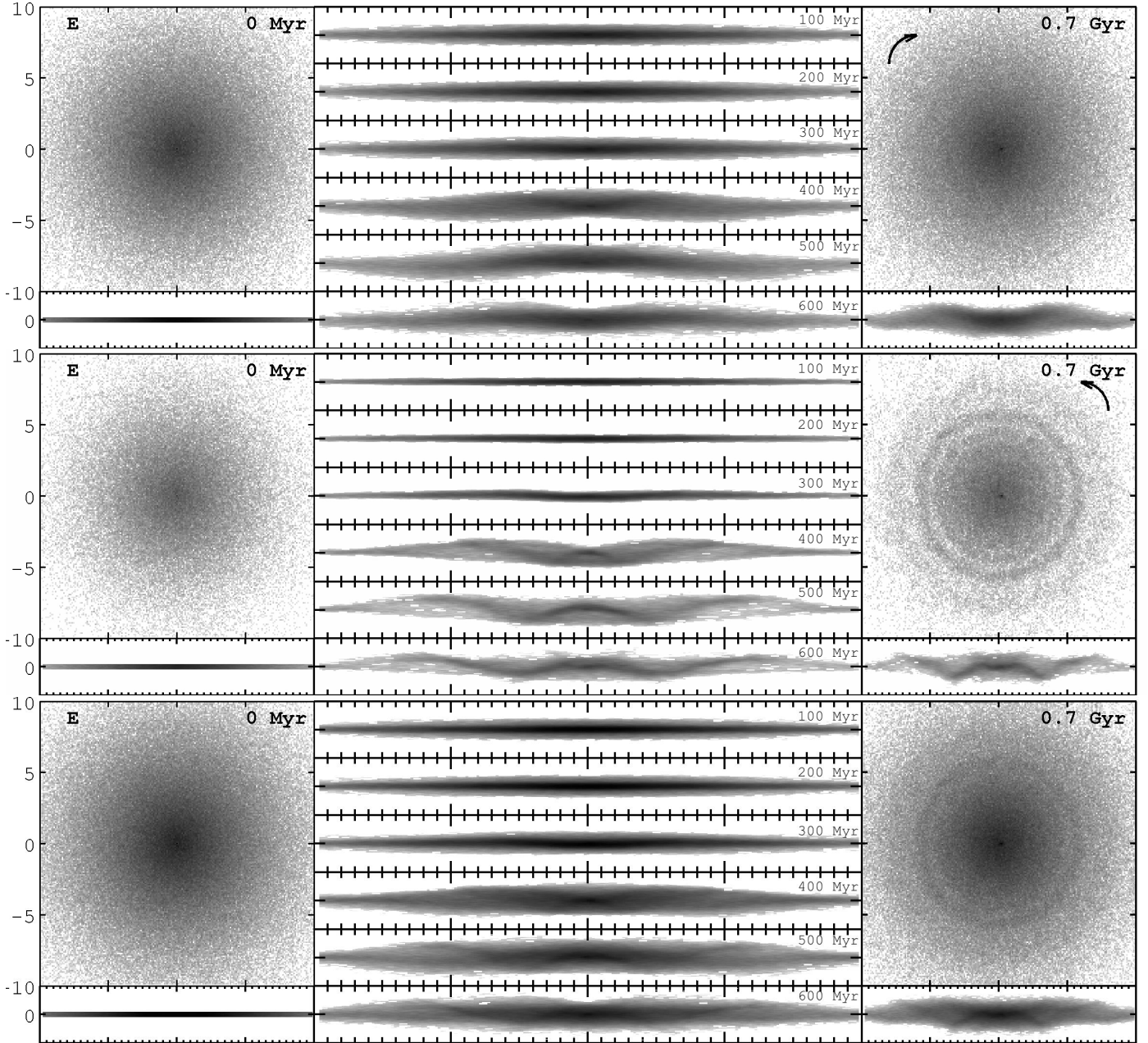
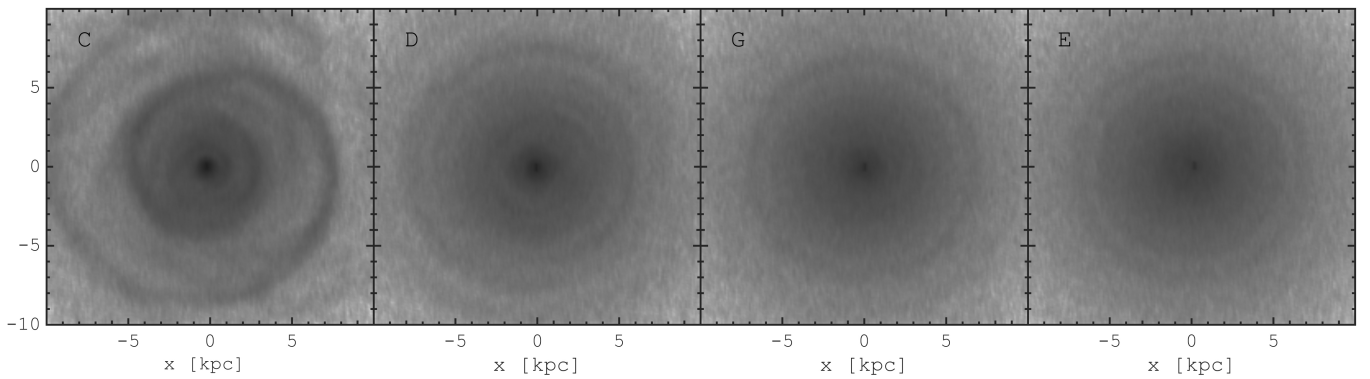**Fig. 6.** As in Fig. 5, but for model E ($Q_{\mathrm{eff}}(R = R^*) = 1.8$).

Fig. 7. Total stellar surface density distribution in the galactic disk at 700 Myr for the four models with counterrotation. *From left to right*: C ($Q_{\mathrm{eff}}(R = R^*) = 0.8$), D ($Q_{\mathrm{eff}}(R = R^*) = 1.0$), G ($Q_{\mathrm{eff}}(R = R^*) = 1.5$), E ($Q_{\mathrm{eff}}(R = R^*) = 1.8$). Each image is 20 kpc across.
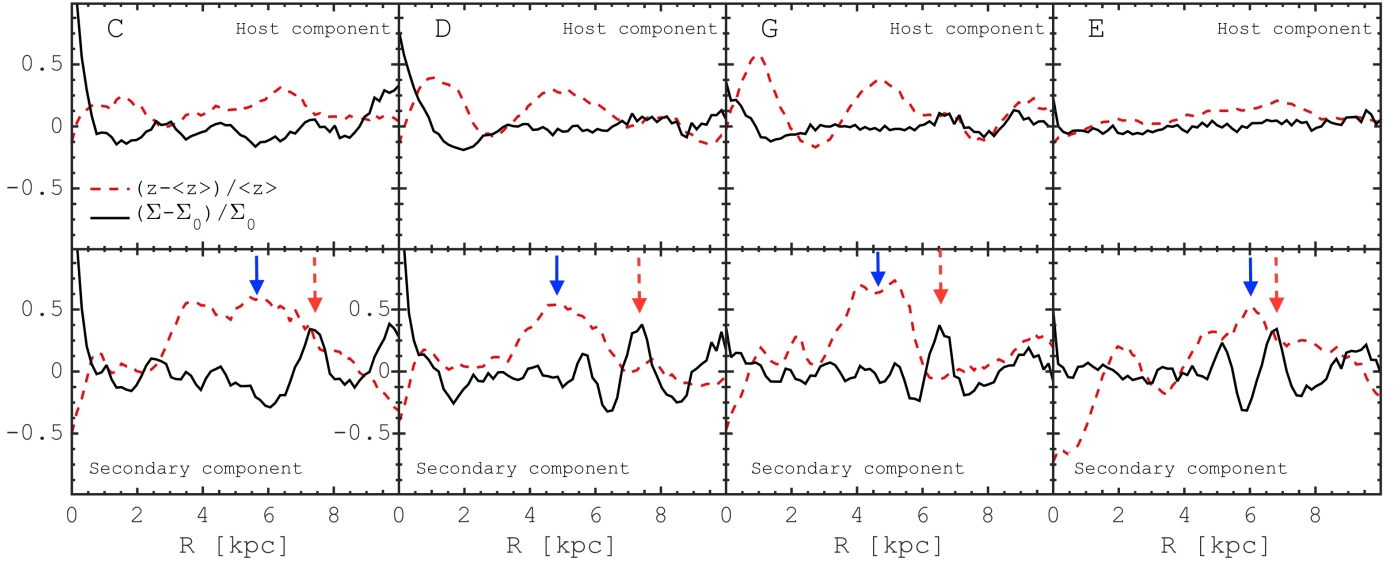
Fig. 8. Radial profiles of relative perturbations of the disk thickness (dashed red line) and surface density (solid black line) for the four models with counterrotation (same models as in Fig. 7). *Top row* shows the data for the host component, *bottom row* for the secondary component of the simulated galaxy. Blue solid vertical arrows show the position of the bending wave peak. Red dashed vertical arrows show the location of the most prominent ring structure (see also Fig. 7). In model C, rings are present, but they are connected with the one-armed spiral structure. In all models the ring structure is strongest in the outer parts of the bending wave.

where $\sigma^2 = \sigma_R^2 + \sigma_\varphi^2 + \sigma_z^2$. This parameter measures in dimensionless form the strength of counterrotation, in terms of a kinetic energy ratio.

In Fig. 10 we plot the evolved mean velocity dispersion ratio $\langle\sigma_z/\sigma_R\rangle$ (at $\approx$600–800 Myr) as a function of the kinetic energy ratio ε (see Eq. (8)) for all the models that we have investigated. Figure 10 shows a reasonable correlation $\varepsilon - \langle\sigma_z/\sigma_R\rangle$, although significant scatter is present:

$$\langle\sigma_z/\sigma_R\rangle \approx \begin{cases} 1.6\varepsilon + 0.4\,, \varepsilon \le 0.5 \\ 1.1\,, \varepsilon > 0.5. \end{cases} \qquad (9)$$

This interpolating formula covers all the models considered in the present paper, including models Kb and Kc, characterized by initial vertical-to-radial velocity dispersion ratio of 0.55 and 0.4.

4. Discussion

Here we briefly comment on possible consequences that may be relevant to observed galaxies. We have shown that, especially as a result of thickening and heating induced by bending instabilities, counterrotation can give rise to significant evolution on a relatively short time scale (200–300 Myr). This evolution is fast and is not to be confused with the results of other secular processes in galaxies (Debattista et al. 2006) and slow Jeans-related phenomena that may be difficult to disentangle from numerical relaxation effects (Sellwood 2013). We argue that such fast evolution is expected to take place independently of the formation scenario that may have led to the "initial" counterrotating system and is likely to hold even in different situations, for example in the case when the secondary counterrotating disk is gaseous; of course, different physical situations would require the consideration of other processes, such as star formation efficiency and depletion time, and new simulations should be run to confirm the general features of the evolutionary process or to identify specific phenomena related to the presence of gaseous components.

Our simulations point to final states characterized by high values of the velocity dispersion ratio for both disk components.

It would be interesting to gather independent observational constraints on this parameter for individual objects. In turn, this quantity plays an important role in determining the projected line-of-sight velocity dispersion $\sigma_{\rm los}$ and in the disk-halo decomposition of rotation curves.

The acquisition of a counterrotating component may be more frequent than generally believed. In turn, the presence of a secondary counterrotating component at a given epoch may be hard to detect for a number of reasons, not only because the resulting evolution is expected to be fast but especially because a relatively light counterrotating component can easily escape observations. Thus the mechanism of vertical disk heating discussed in this paper may have been overlooked. Certainly, from the theoretical point of view, its occurrence and its impact should be studied further, because in the past little attention has been paid to it.

5. Conclusions

In this work we have examined the evolution of two-component collisionless galactic disks by means of numerical simulations. In the presence of counterrotation, bending waves have been found to be excited (two-stream instability). The most prominent and, in a sense, surprising result is that evolution proceeds by effects that change the three-dimensional structure of the system:

– In the case of counterrotating disks, gravitational instabilities in the disk plane are less effective (with respect to the case of two co-rotating disks with similar structure). The instability in systems with counterrotation develops mostly in the vertical direction. Strong bending instabilities are excited and lead to a significant increase of the vertical-to-radial velocity dispersion ratio $\langle\sigma_z/\sigma_R\rangle$. In contrast to other relaxation processes in one-component disks, the effects noted in this paper for two-component counterrotating disks occur on the short dynamical time-scale of about 400 Myr.
– The mean value of the velocity dispersion ratio in the disk is found to increase up to values close to unity for both counterrotating components of the disk. The effect is stronger when
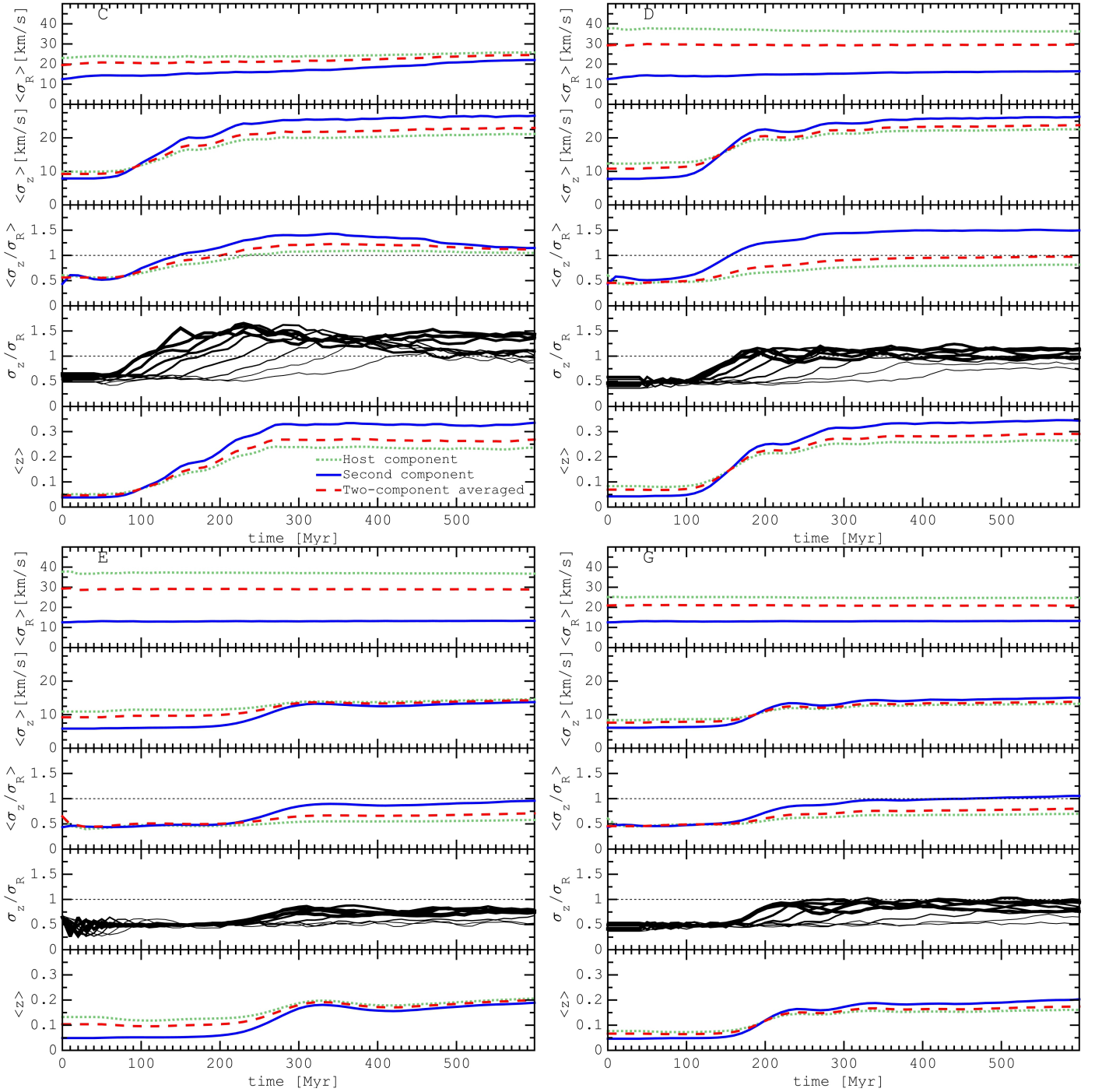
Fig. 9. Evolution of the disk parameters, in the same format as in Fig. 4, for four models with counterrotation. Black lines in the fourth frame of each of the four panels show the evolution of two-component averaged values of the velocity dispersion ratio σ_z/σ_R at various radii (line thickness decreases with radial distance from the center).

the free energy associated with counterrotation is larger and then the effects appear to saturate at $\langle\sigma_z/\sigma_R\rangle \approx 1$. For some parameter regimes, in the central regions the velocity dispersion ratio can reach values even higher than unity ≈ 1.2–1.5 (see Fig. 10).

– The final velocity dispersion ratio is found to change with radius for both counterrotating components (see Figs. 9 and 10).

– We found that density-wave ring-like structures are driven by bending instabilities in galaxies with counterrotation. We clearly demonstrate that the outer edge of the bending

wave is associated with the rings seen in the face-on density maps.

– A correlation has been found between the final "equilibrium" velocity dispersion ratio $\langle\sigma_z/\sigma_R\rangle$ and a dimensionless parameter ε that we have introduced to characterize the strength of counterrotation. Namely, we found that the $\langle\sigma_z/\sigma_R\rangle$ increases from 0.4 up to 1.0–1.2 in the range $\varepsilon = 0$–0.5. At larger values of the counterrotation strength (>0.5) the resulting velocity dispersion ratio saturates around unity.

– We argue that vertical disk heating due to bending waves induced by counterrotation may be a relatively common
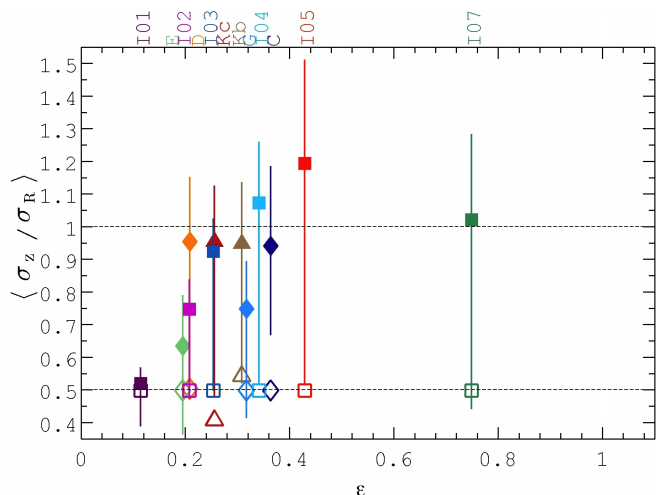
Fig. 10. Mean value of the velocity dispersion ratio $\langle \sigma_z/\sigma_R \rangle$ as a function of ε at $\approx$600–800 Myr (filled symbols) in various models; initial $\langle \sigma_z/\sigma_R \rangle$ values are shown by open symbols. Different symbols correspond to different groups of models in Table 1: diamonds for models C, D, E, G; squares for models I01, I02, I03, I04, I05, I07; triangles for models Kb and Kc. Model names are shown above the plot. Vertical error bars correspond to the range of the velocity dispersion ratio, which changes with radius in the final evolved state.

heating mechanism. Indeed the direct observation of counterrotation may be rare just because the resulting evolution is fast (as shown in this paper) and because relatively light counterrotating disks may escape observations.

References

Algorry, D. G., Navarro, J. F., Abadi, M. G., et al. 2014, MNRAS, 437, 3596
Araki, S. 1987, AJ, 94, 99
Aumer, M., Binney, J., & Schönrich, R. 2016, MNRAS, 462, 1697
Barnes, J., & Hut, P. 1986, Nature, 324, 446
Benson, A. J., Lacey, C. G., Frenk, C. S., Baugh, C. M., & Cole, S. 2004, MNRAS, 351, 1215
Bershady, M. A., Martinsson, T. P. K., Verheijen, M. A. W., et al. 2011, ApJ, 739, L47
Bertin, G. 2014, in Dynamics of Galaxies, 2nd edn. (New York: Cambridge University Press)
Bertin, G., & Casertano, S. 1982, A&A, 106, 274
Bertin, G., & Cava, A. 2006, A&A, 459, 333
Bertin, G., & Lin, C. C. 1996, in Spiral structure in galaxies: a density wave theory (Cambridge, MA: The MIT Press)
Bertin, G., & Mark, J. W.-K. 1980, A&A, 88, 289
Bertola, F., & Corsini, E. M. 1999, in Galaxy Interactions at Low and High Redshift, eds. J. E. Barnes, & D. B. Sanders, IAU Symp., 186, 149
Bluck, A. F. L., Conselice, C. J., Buitrago, F., et al. 2012, ApJ, 747, 34
Boardman, N. F., Weijmans, A., van den Bosch, R. C. E., et al. 2016, MNRAS, 460, 3029
Coccato, L., Morelli, L., Corsini, E. M., et al. 2011, MNRAS, 412, L113
Coccato, L., Fabricius, M., Morelli, L., et al. 2015, A&A, 581, A65
Combes, F., & Arnaboldi, M. 1996, A&A, 305, 763
Comins, N. F., Lovelace, R. V. E., Zeltwanger, T., & Shorey, P. 1997, ApJ, 484, L33
Conselice, C. J. 2014, in Multi-Spin Galaxies, eds. E. Iodice, & E. M. Corsini, ASP Conf. Ser., 486, 85

Conselice, C. J., Rajgor, S., & Myers, R. 2008, MNRAS, 386, 909
Corsini, E. M. 2014, in Multi-Spin Galaxies, eds. E. Iodice, & E. M. Corsini, ASP Conf. Ser., 486, 51
Davis, T. A., Alatalo, K., Sarzi, M., et al. 2011, MNRAS, 417, 882
Debattista, V. P., Mayer, L., Carollo, C. M., et al. 2006, ApJ, 645, 209
Faucher-Giguère, C.-A., Kereš, D., & Ma, C.-P. 2011, MNRAS, 417, 2982
Font, A. S., Navarro, J. F., Stadel, J., & Quinn, T. 2001, ApJ, 563, L1
Friedli, D. 1996, A&A, 312, 761
Gadotti, D. A., & de Souza, R. E. 2005, ApJ, 629, 797
Gerssen, J., & Shapiro Griffin, K. 2012, MNRAS, 423, 2726
Griv, E. 2011, MNRAS, 415, 1259
Gulati, M., & Deep Saini, T. 2016, ArXiv e-prints [arXiv:1602.07169]
Hänninen, J., & Flynn, C. 2004, A&A, 421, 1001
Jenkins, A., & Binney, J. 1990, MNRAS, 245, 305
Katkov, I., Chilingarian, I., Sil'chenko, O., Zasov, A., & Afanasiev, V. 2011, Baltic Astron., 20, 453
Katkov, I. Y., Sil'chenko, O. K., & Afanasiev, V. L. 2013, ApJ, 769, 105
Katkov, I. Y., Sil'chenko, O. K., Chilingarian, I. V., Uklein, R. I., & Egorov, O. V. 2016, MNRAS, 461, 2068
Khoperskov, A. V., Zasov, A. V., & Tyurina, N. V. 2001, Astron. Rep., 45, 180
Khoperskov, A., Bizyaev, D., Tiurina, N., & Butenko, M. 2010, Astron. Nachr., 331, 731
Khoperskov, S. A., Khoperskov, A. V., Khrykin, I. S., et al. 2012a, MNRAS, 427, 1983
Khoperskov, S. A., Shustov, B. M., & Khoperskov, A. V. 2012b, Astron. Rep., 56, 664
Khoperskov, A. V., Khoperskov, S. A., Zasov, A. V., Bizyaev, D. V., & Khrapov, S. S. 2013, MNRAS, 431, 1230
Khoperskov, S. A., Moiseev, A. V., Khoperskov, A. V., & Saburova, A. S. 2014a, MNRAS, 441, 2650
Khoperskov, S. A., Vasiliev, E. O., Khoperskov, A. V., & Lubimov, V. N. 2014b, J. Phys. Conf. Ser., 510, 012011
Khoperskov, S. A., Vasiliev, E. O., Ladeyschikov, D. A., Sobolev, A. M., & Khoperskov, A. V. 2016, MNRAS, 455, 1782
Kulsrud, R. M., Mark, J. W. K., & Caruso, A. 1971, Ap&SS, 14, 52
Lacey, C. G. 1984, MNRAS, 208, 687
Lacey, C. G., & Ostriker, J. P. 1985, ApJ, 299, 633
Laughlin, G., Korchagin, V., & Adams, F. C. 1997, ApJ, 477, 410
Lin, C. C., & Shu, F. H. 1966, Proc. National Academy of Science, 55, 229
Lovelace, R. V. E., Jore, K. P., & Haynes, M. P. 1997, ApJ, 475, 83
Maciejewski, W. 2006, MNRAS, 371, 451
Mark, J. W.-K. 1976, ApJ, 206, 418
Marochnik, L. S., & Suchkov, A. A. 1971, Astrophys. Lett., 9, 37
Merritt, D., & Sellwood, J. A. 1994, ApJ, 425, 551
Minchev, I., & Quillen, A. C. 2006, MNRAS, 368, 623
Moiseev, A. V. 2012, Astrophys. Bull., 67, 147
Moiseev, A. V., Smirnova, K. I., Smirnova, A. A., & Reshetnikov, V. P. 2011, MNRAS, 418, 244
Pizzella, A., Morelli, L., Corsini, E. M., et al. 2014, A&A, 570, A79
Poliachenko, V. L., & Shukhman, I. G. 1977, Sov. Astron. Lett., 3, 134
Quach, D., Dyda, S., & Lovelace, R. V. E. 2015, MNRAS, 446, 622
Raha, N., Sellwood, J. A., James, R. A., & Kahn, F. D. 1991, Nature, 352, 411
Reshetnikov, V. P., & Sotnikova, N. Y. 2000, Astron. Lett., 26, 277
Rodionov, S. A., & Sotnikova, N. Y. 2013, MNRAS, 434, 2373
Romeo, A. B., & Falstad, N. 2013, MNRAS, 433, 1389
Romeo, A. B., & Wiegert, J. 2011, MNRAS, 416, 1191
Rubin, V. C. 1994, AJ, 108, 456
Rubin, V. C., Graham, J. A., & Kenney, J. D. P. 1992, ApJ, 394, L9
Sackett, P. D., Rix, H.-W., Jarvis, B. J., & Freeman, K. C. 1994, ApJ, 436, 629
Saha, K., Tseng, Y.-H., & Taam, R. E. 2010, ApJ, 721, 1878
Sellwood, J. A. 1996, ApJ, 473, 733
Sellwood, J. A. 2013, ApJ, 769, L24
Sellwood, J. A., & Merritt, D. 1994, ApJ, 425, 530
Shapiro, K. L., Gerssen, J., & van der Marel, R. P. 2003, AJ, 126, 2707
Sil'chenko, O. K., Moiseev, A. V., & Afanasiev, V. L. 2009, ApJ, 694, 1550
Sotnikova, N. Y., & Rodionov, S. A. 2005, Astron. Lett., 31, 15
Spitzer, Jr., L., & Schwarzschild, M. 1951, ApJ, 114, 385
Thakar, A. R., & Ryden, B. S. 1996, ApJ, 461, 55
Toomre, A. 1964, ApJ, 139, 1217
Toomre, A. 1966, Geophys. Fluid Dyn., 66, 111
Toomre, A. 1981, in Structure and Evolution of Normal Galaxies, eds. S. M. Fall, & D. Lynden-Bell, 111
van der Kruit, P. C., & de Grijs, R. 1999, A&A, 352, 129
van der Kruit, P. C., & Freeman, K. C. 2011, ARA&A, 49, 301
van Driel, W., & Buta, R. 1993, PASJ, 45, L47
Verheijen, M. A. W., Bershady, M. A., Andersen, D. R., et al. 2004, Astron. Nachr., 325, 151
Whitmore, B. C., McElroy, D. B., & Schweizer, F. 1987, ApJ, 314, 439